Neurosci. Bull. June, 2019, 35(3):389–400
https://doi.org/10.1007/s12264-019-00370-z

www.neurosci.cn
www.springer.com/12264

METHOD

High-Throughput Automatic Training System for Spatial Working Memory in Free-Moving Mice

Shimin Zou[1,2] · **Chengyu Tony Li**[1,2]

Received: 14 August 2018 / Accepted: 12 December 2018 / Published online: 11 April 2019

Abstract Efficient behavioral assays are crucial for understanding the neural mechanisms of cognitive functions. Here, we designed a high-throughput automatic training system for spatial cognition (HASS) for free-moving mice. Mice were trained to return to the home arm and remain there during a delay period. Software was designed to enable automatic training in all its phases, including habituation, shaping, and learning. Using this system, we trained mice to successfully perform a spatially delayed nonmatch to sample task, which tested spatial cognition, working memory, and decision making. Performance depended on the delay duration, which is a hallmark of working memory tasks. The HASS enabled a human operator to train more than six mice simultaneously with minimal intervention, therefore greatly enhancing experimental efficiency and minimizing stress to the mice. Combined with the optogenetic method and neurophysiological techniques, the HASS will be useful in deciphering the neural circuitry underlying spatial cognition.

Keywords Cognitive functions · Automatic training · Free-moving mice · Working memory · Spatial cognition

✉ Chengyu Tony Li
tonylicy@ion.ac.cn

[1] Institute of Neuroscience, State Key Laboratory of Neuroscience, Chinese Academy of Sciences, CAS Center for Excellence in Brain Science and Intelligence Technology, Shanghai Center for Brain Science and Brain-Inspired Technology, Shanghai 200031, China

[2] School of Future Technology, University of Chinese Academy of Sciences, Beijing 100049, China

Introduction

The design of behavioral paradigms plays an important role in the study of cognition [1]. Suitable animal models and reliable behavioral paradigms are necessary for understanding cognitive functions, such as working memory [2, 3], decision-making [4, 5] and spatial navigation [6–8]. A well-designed behavioral paradigm is not only important for basic research but also useful for preclinical studies, including mechanistic studies of brain diseases and drug screening [9–11]. An ideal behavioral system should be automatic [12], easy to scale up, and compatible with neural-circuitry technologies, including optogenetics [13], chemogenetics [14] and imaging methods [15].

Previously, many automatic behavior-training systems have been developed, for example, in studies of operant conditioning [16], visual-task performance [17–19], odor-based behaviors [20], pain sensitivity [21, 22], freezing behavior during fear conditioning [23, 24], home-cage phenotyping [25–27], anxiety [28], diurnal rhythms [29], and social behavior [30–32]. Automatic training systems have also been used in multiple behavioral domains, including memory assessment [33], operant learning [34], training limb function [35], and other cognitive tasks requiring attention, memory, and decision-making in free-moving rats [36, 37] and mice [38, 39]. Moreover, such systems have also worked well in dissecting neural-circuitry mechanisms underlying cognitive behaviors [36, 40–42]. In this study, we sought to establish an automatic and high-throughput training system for spatial working memory in rodents.

Spatial working memory is the function of actively holding spatial information in the brain before a subject reaches a behavioral goal [2, 43–46]. Spatial working memory links information from the past, the current goal,

and the immediate act and is thus essential for daily life and survival [40–43]. Deficits in spatial working memory have been consistently observed in patients with many brain disorders, such as schizophrenia [47]. Therefore, a rodent spatial working memory paradigm is useful for both understanding its related neuronal mechanisms [40, 48–53] and serving as an endophenotype in preclinical studies [54]. Previously, an automatic training system based on delayed alternation between two choice arms was developed [55]; in this system, rodents are usually trained with a delayed nonmatch to sample (DNMS) task or a delayed alteration task. We thus added more goal arms to extend the flexibility of the behavioral design.

We designed a high-throughput automatic training system for spatial cognition (HASS) for spatial behaviors in free-moving mice. Adopting explicit step-by-step training procedures, we trained mice to perform a spatial DNMS task in the HASS. Mice reached stable correct rates within a short training period. HASS could be a useful tool in studying neural-circuitry mechanisms underlying spatial cognitive functions.

Materials and Methods

Subjects

Male adult C57BL/6 mice (Shanghai Laboratory Animal Center, CAS, Shanghai, China) aged 8–16 weeks before the start of training were used for all experiments. Mice were group-housed (4–6/cage) in the animal facility of the Institute of Neuroscience and were maintained on a 12-h light-dark cycle. Other than during behavioral training, all mice were given *ad libitum* access to food and water. During the training process, the water supply was restricted. Mice could obtain water only during and immediately after training. The water supply after training was set to maintain 80% of their pre-training bodyweight. All procedures were approved by the Animal Care and Use Committee of the Institute of Neuroscience at the Chinese Academy of Sciences in Shanghai, China.

Behavioral Setups

The HASS was composed of a maze, detecting units, door-controlling units, rewarding units, and Arduino-based (https://store.arduino.cc/usa/mega-2560-r3) hardware-controlling and data-acquisition units (Fig. 1A). All peristaltic pumps and steering engines were controlled by Arduino-based processors (Arduino MEGA 2560) and customized software.

The white acrylic maze was amerge of a T- and a Y-maze (Fig. 2A), including one home-arm and four goal arms. Within the four goal arms, two arms at 180° were termed "T" arms, whereas the other arms at a smaller angle (60°) were termed "Y" arms. Each arm was connected to a door-controlling unit, a rewarding unit, and an infrared detecting unit. A round acrylic plate embedded in the central area that was controlled by the steering engine could rotate by pseudorandom angles (90°, 120°, 150°, or 180°) to remove traces of a previous visit during the delay. The details for the maze can be found in CAD files in the supplementary materials and the GitHub website (https://github.com/Caticorn/CAD-acrylic-five-arm-maze).

A door-controlling unit was composed of a servo [Futaba S3003 (https://www.towerhobbies.com/cgi-bin/wti0001p?123&I=FUTM0031&P=3), c1 in Fig. 2B, D], a metal rudder arm (25 Tooth, 37 mm, c2 in Fig. 2B, D), and an acrylic door (Fig. 2B). The steering engine was fixed under the floor of each arm (Fig. 2B, D) and connected to a rudder arm through a hole in the floor. The door, fixed to the rudder arm, could be open or closed when the servo, controlled by an Arduino board, rotated by 0° or 90°. There were two door-controlling units for the home arm and one for each goal arm. In addition to door-controlling units, another servo was fixed under the round acrylic plate (Fig. 2A, D) through the original X-shaped servo arm (38 mm) to rotate the central floor by a pseudorandom angle (90°, 120°, 150°, or 180°) during the delay. In summary, seven servos (six for door control and one for rotating the central plate), six acrylic doors, one X-shaped servo arm, and six metal rudder arms were needed for each maze.

A pair of infrared elements, an infrared LED (wavelength: 940 nm, $\Phi = 5$ mm, d1 in Fig. 2C, D) and an infrared sensor ($\Phi = 5$ mm, d2 in Fig. 2C, D), was separately embedded on the two sidewalls of each arm as detection units. The infrared sensor detected animal motion when a passing mouse blocked the infrared beam. Mouse-passage events were detected and sent to the Arduino board, which logged the event and triggered the next process according to the training protocol. In each maze, there were five infrared LEDs and five paired infrared sensors.

At the end of each arm, a metal water port with a blunt tip (r1 in Fig. 2D) was connected to a peristaltic pump (Runzei RZ1020A or Kamoer KFS-HB2B03R, r3 in Fig. 2D), which pumped water from the connected bottle (r2 in Fig. 2D) to the water port through tubes (15–20 cm, r4 in Fig. 2D) under the control of the Arduino board [17–19]. The volume of the water reward was controlled by the duration of the digital output signal. The peristaltic pumps indifferent arms of the same system were adjusted to the same flow rate to balance the reward size in each goal arm. In summary, there were five peristaltic pumps, five bottles, and ten water tubes in each system.

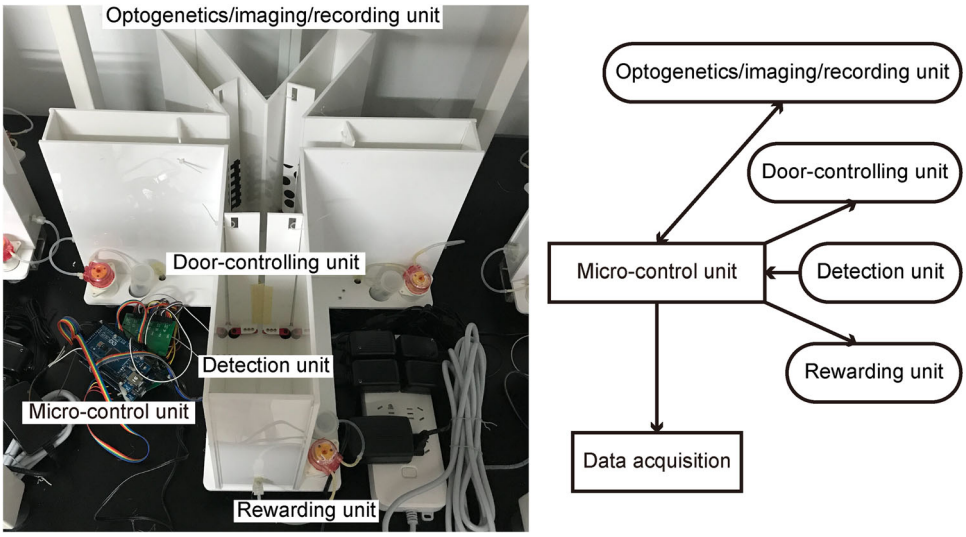

Fig. 1 Photograph (left) and schematic (right) of the high-throughput automatic training system for spatial cognition. Arrows represent the direction of flow of hardware states and control signals.

All the above units were connected to the Arduino boards. In the current version, two Arduino boards were used: the motherboard accepted analog input from the infrared sensors and sent control signals (digital output) to peristaltic pumps and a secondary board, which then sent control signals [pulse width modulation (PWM) output] directly to servos based on the signal from the motherboard (Fig. 3A). When a mouse entered an arm (Fig. 3B①), the infrared sensor detected it and sent a signal to the Arduino board (Fig. 3B②, analog signal lower than threshold); then, according to the task phase, the processor sent a control PWM signal to the servo to control the opening or closing of the corresponding doors (Fig. 3B③) and a digital signal to the peristaltic pump to control water delivery (Fig. 3B④).

During training, the event information and the timestamps were sent back to a computer *via* a USB-simulated serial-port interface and recorded by a customized JAVA program, as in Ref. [20]. The saved information included the arm-indexes of the sample and choice arms, the transpassing of the mouse, the on/off events of the peristaltic pump, and the start/end times for a given trial. The source code for behavioral training and data acquisition is available in the supplementary materials and the GitHub website (code for hardware control at https://github.com/Caticorn/high-throughput-automatic-training-system-for-spatial-cognition, and code for behavioral data analysis at https://github.com/Caticorn/DNMS-behavior-analysis).

A wide-angle camera above the maze monitored the motion of mice during training. Optogenetics, calcium-imaging, and recording units could be added as extended modules when needed. For optogenetic extended units, the laser could be connected to the digital pin of the motherboard (Arduino MEGA2560) and controlled by a TTL signal (timestamp) to temporally and specifically switch on or off during various training durations. The processor could also send a time stamp (TTL signal) to synchronize imaging and recording units.

Behavioral Paradigm

In the spatial DNMS task, each trial is composed of a sample and a choice phase, with a delay offixed or varying duration between the two phases (Figs. 4, 5). A sample arm is open at the start of the sample phase. The mouse runs from the home arm to the sample arm to receive a small amount of water reward (~3.5 μL, 60 ms in duration). Then, the mouse returns to the home arm. The home-arm doors are then closed, and the mouse remains there for the entire delay duration. During the delay period, the rotatory plate embedded in the center is rotated by a pseudorandom angle. Two goal arms are opened in the choice phase: one is the same as the sampled arm, and the other is non-matched to the sampled arm (target). To simplify the task statistics, only the combination of "Y–Y" or "T–T" arms were used in this study. That is, after a sample trial of a particular "T" arm, in the choice phase only two "T" arms are opened. In "Y" arm sample trials, only the "Y" arms are opened. After the delay, the home-arm door is opened, and the mouse needs to decide between two goal arms. In the DNMS task, if the mouse first enters the non-matched arm, the trial is regarded as a "hit" and triggers water delivery (~5.5 μL, 100 ms) in the chosen arm. Furthermore, the mouse then returns to the home-arm to receive an additional 3.5 μL of water at the end of that arm. Conversely, if the mouse enters the matched arm first, the trial is defined as a "false" trial and no water reward is delivered in any arm. A mouse is not specifically punished after a false choice except for the lack of a reward. A predetermined intertrial interval is then applied when the mouse is waiting in the home arm.

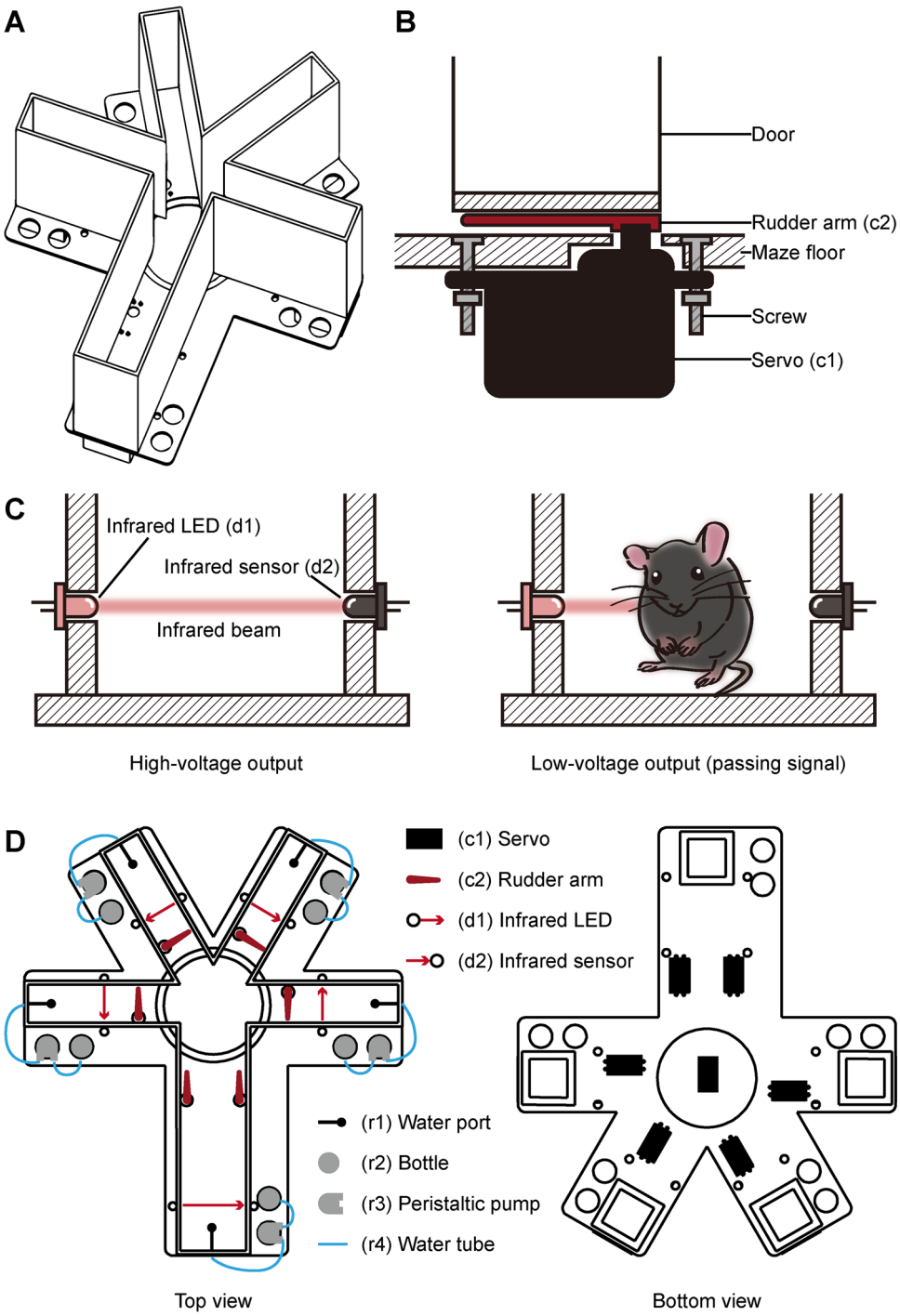

Fig. 2 Components of the HASS. **A** Isometric view of the radial five-arm maze. **B** Schematic of a door-controlling unit. **C** Schematic of the passage-detection unit. Left: infrared sensor detects the infrared beam emitted from the infrared LED and sends a high-voltage signal to the Arduino-based processor. Right: when a passing mouse blocks the infrared beam, the infrared sensor outputs a low-voltage signal. **D** Locations of various components.

Behavioral Training

Water Restriction

Once training started, the mice could drink water only during and immediately after a task, and the minimum water intake per day was 0.6 mL to keep the animals healthy. Mice were weighed daily and maintained at 80% of the pre-training level.

Habituation

Mice were habituated for two days in the training system at the beginning of the training process (Fig. 6). On each day of habituation, the mouse was gently and individually put in the home arm and allowed to freely explore the maze with all doors open for one hour. After daily habituation, mice were weighed and supplied with water in their home

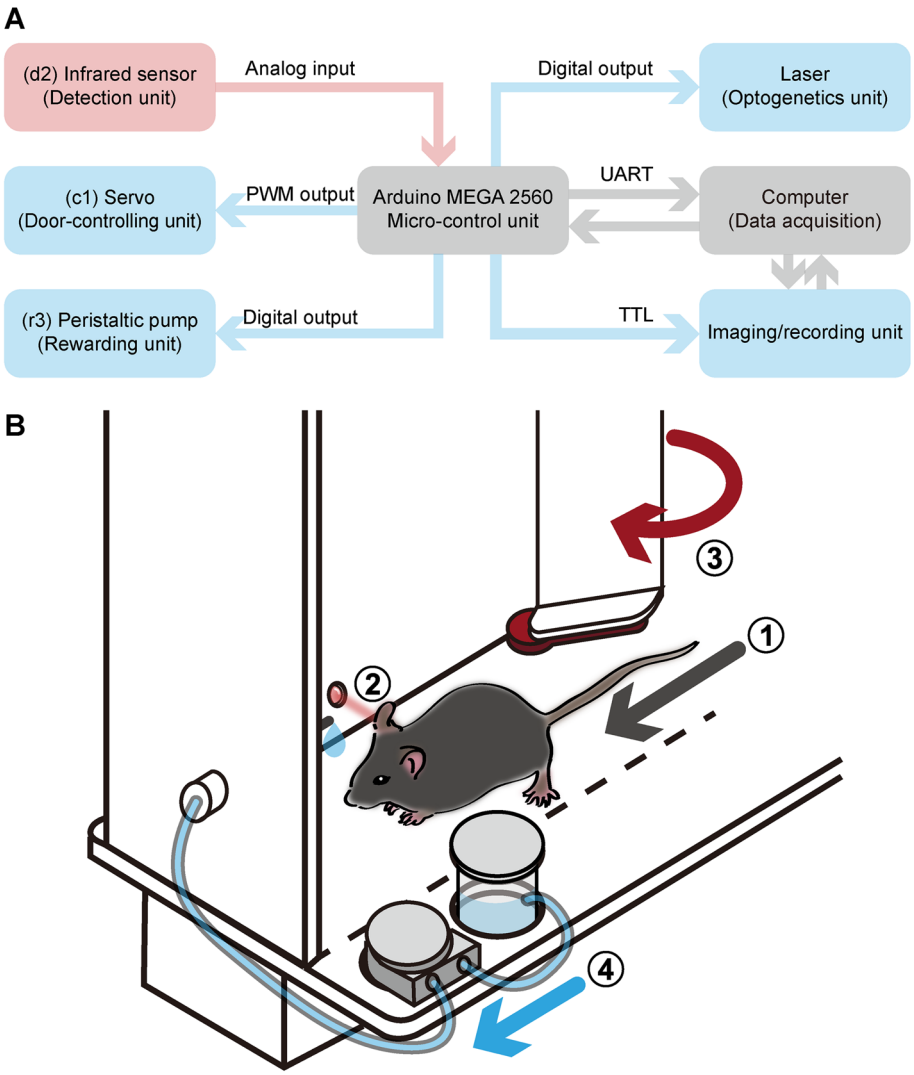

Fig. 3 The HASS workflow. **A** Schematic of the connections and communication in the apparatus. **B**① When the mouse passes a sensor (gray arrow represents the direction of mouse movement), ② the infrared beam is blocked, and ③ the door is closed (or opened) by a servo (red arrow represents the direction of door rotation); then, ④ water is delivered (blue arrow represents the direction of water flow) by a peristaltic pump.

cage for 10min. No water was given from the water ports within the maze in this step.

Automatic Shaping

For the subsequent 2–5 days, mice underwent behavioral shaping (Fig. 6). Each shaping trial consisted of a sample and a choice phase, with or without a delay period in between (Fig. 7A). One of the four arms was open pseudo randomly in the sample phase. Then, the mouse was expected to explore the sample arm to obtain water (3.5 μL) at the end of the arm. After the mouse returned to the home arm, water was delivered at the end of the home arm (3.5 μL) to teach mice the "come-back" rule: return to the home arm after exploring a goal arm. Then, another arm was opened as the choice arm (nonmatched arm) in the choice phase. Similar to the task training step, in the shaping phase, only the combination of "Y"–"Y" or "T"–"T" arms was used. During the shaping phase, entering either arm resulted in a water reward (~5.5 μL) in the chosen arm. Mice would also obtain another water reward (3.5 μL) at the end of the home arm after the choice phase.

At the early stage of the shaping phase, there was no delay between the sample and choice phases. Furthermore, the home doors were kept open to prevent the mice from being hit by the closing doors and to minimize the ambient noise. After mice were familiarized with the "come-back" rule and ran sufficiently quickly, the home arms were closed after a mouse returned, and it was kept inside for 5s during the delay period.

After daily shaping steps, the mice were weighed and supplied with water in their home cage for 10 min. Once mice were able to complete 60 shaping trials in 2 h, they commenced training on the DNMS task in the radial five-arm maze.

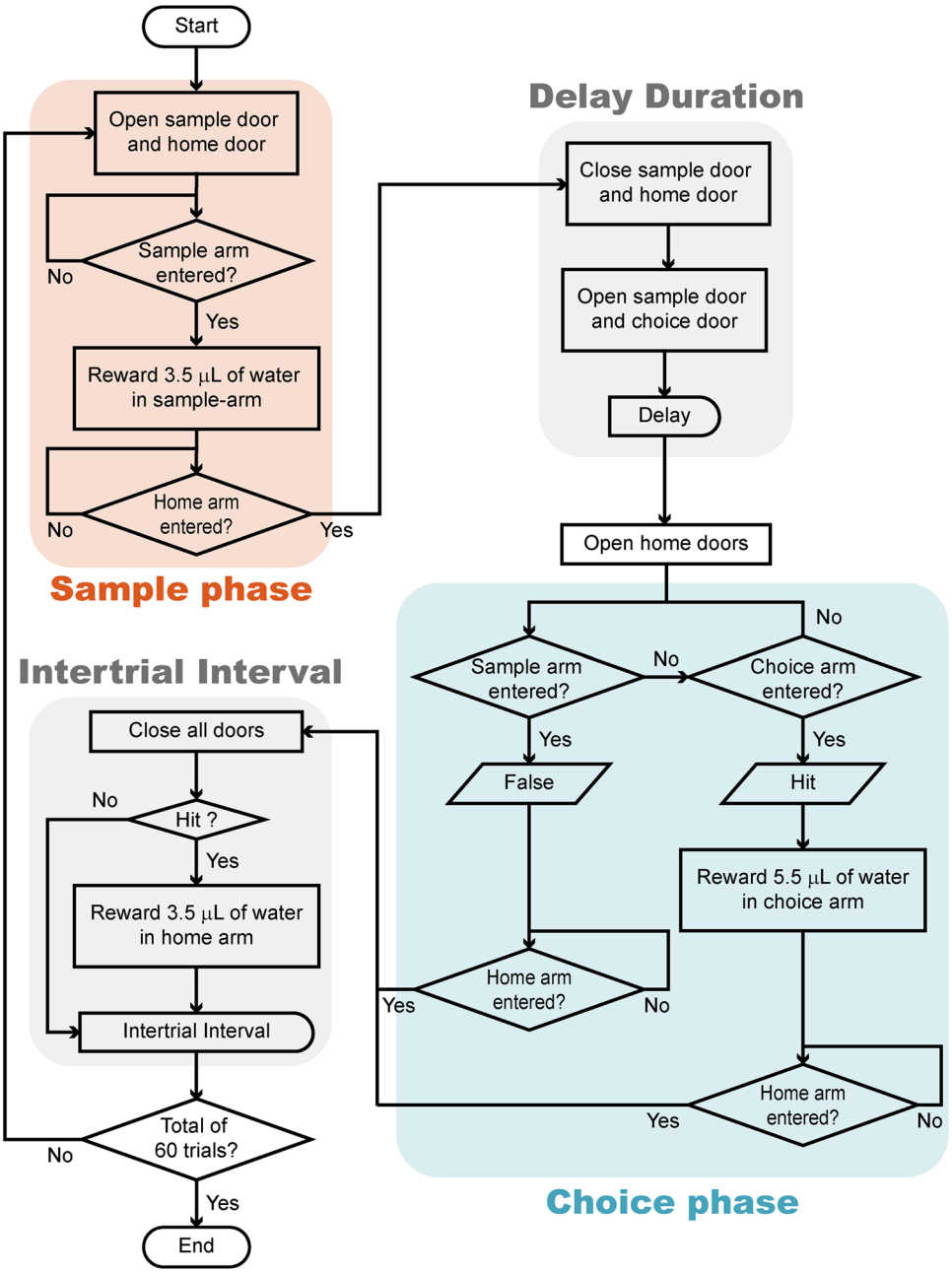

Fig. 4 Flowchart for the spatial DNMS task. Background color indicates trial phase: orange, sample phase; blue, choice phase; gray, delay duration and intertrial interval.

Task Training

As noted above, each DNMS trial consisted of a sample and a choice phase, with a delay period in between (5–60 s, Fig. 8A).

After exploring the sample arm, a mouse returned to the home arm and remained inside during the delay period. Unlike in the shaping phase, water was not delivered in the home arm during the delay period, as the mice were already familiar with the "come-back" rule. The sampled arm (matched arm) and another goal arm (nonmatched arm) opened as two alternative choices. As noted previously, only the combination of "Y–Y" or "T–T" arms was used. Mice could receive a water reward (~5.5 μL) only by first entering the nonmatched arm. To increase the difference between hit and false trials, extra water was delivered in the home arm (~3.5 μL) after a hit trial. Mice were not punished in error trials aside from the lack of a water reward in all arms. A trial ended once the mouse ran back to the home arm after a hit or false choice. Then, the mouse remained in the home arm until the next trial.

In the fixed-delay design, the delay was fixed at 5 s for all trials. In the varied delay design, the delays in the

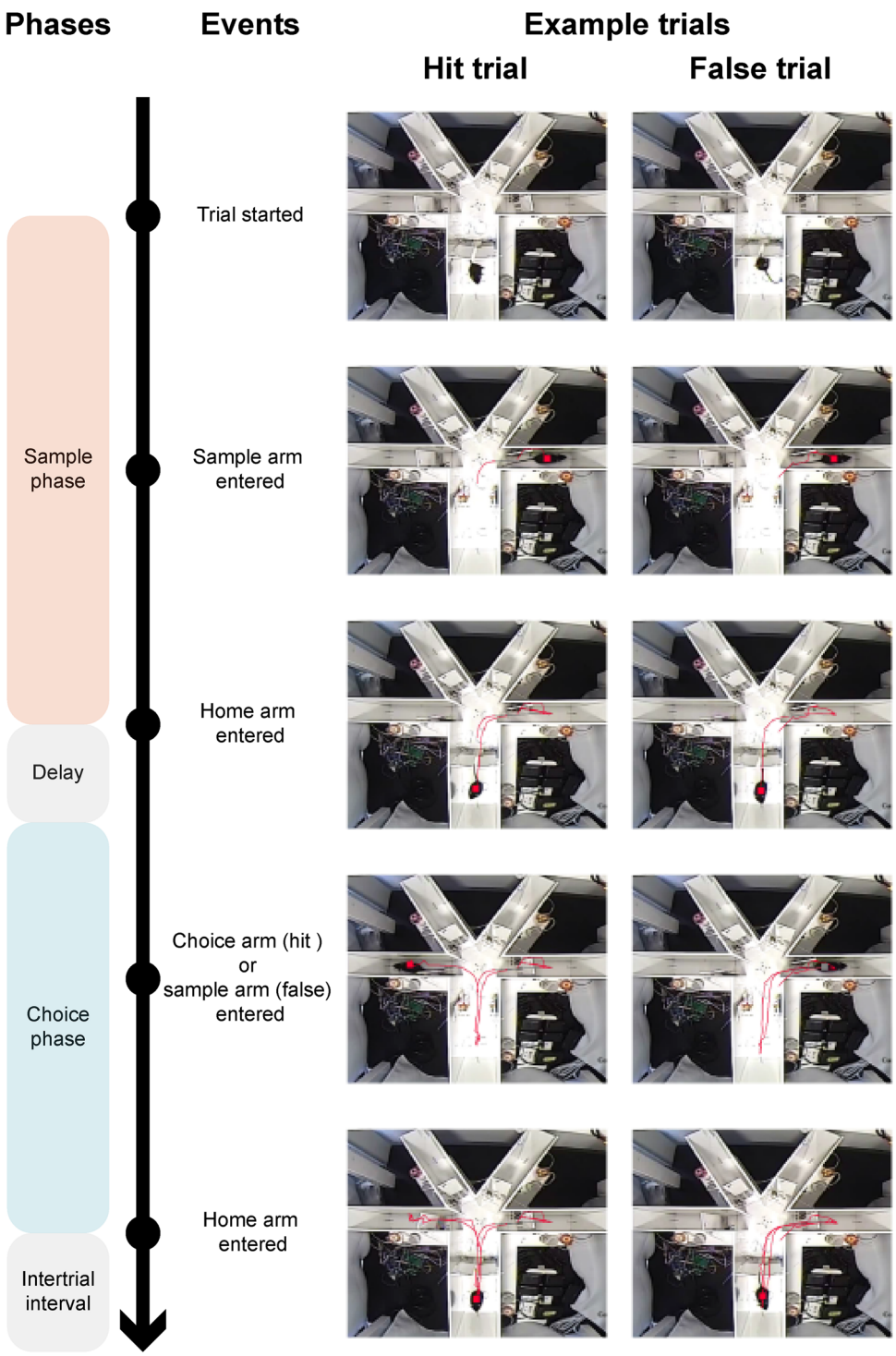

Fig. 5 Example trials. Left, time line marked with trial events. Middle, example of a hit trial. Right, example of a false trial. Red lines represent the trace of the mouse. All images were captured from an example video in the supplementary files.

different trials varied among 5 s, 30 s, and 60 s. The sample and choice arms were pseudo randomly selected trial-by-trial and balanced among all trial conditions ("T–T", "Y–Y", left, right) in one training day.

Behavioral Data Analysis

Typically, the behavioral performance was averaged per day. In the shaping phase, the percentage of choosing the nonmatched arm (R) was defined as follows:

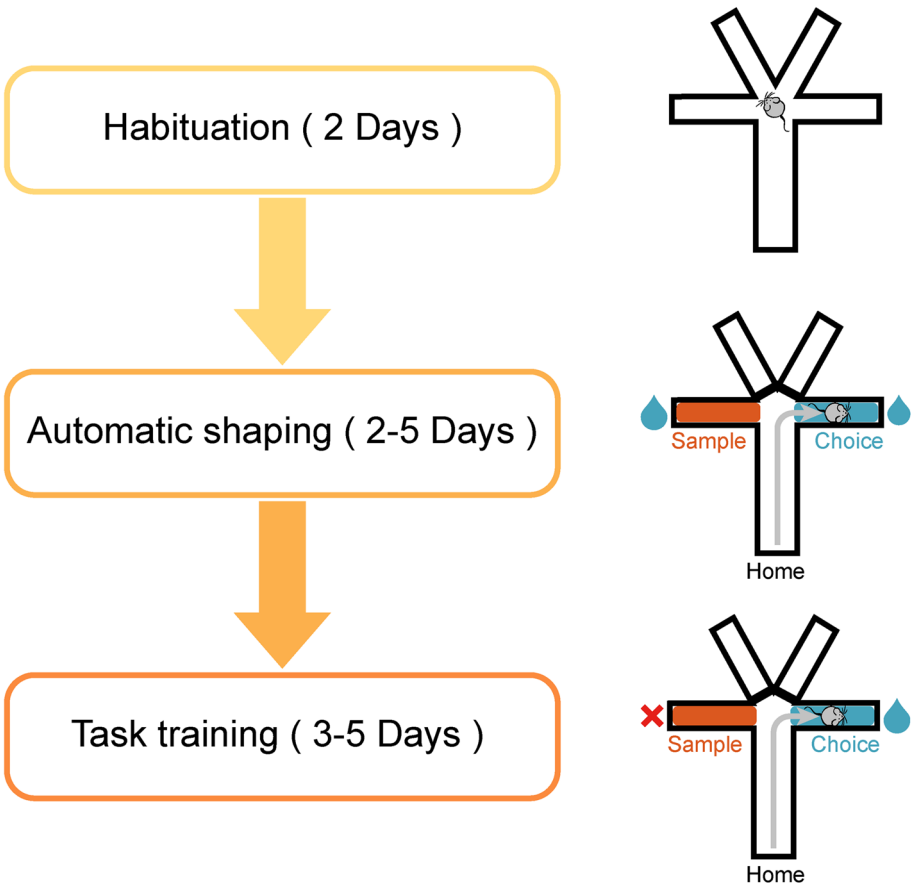

Fig. 6 Left, step-by-step automatic training procedure. Right, corresponding schematics for a mouse in different phases of training. During habituation, all doors are open. During the shaping phase, mice obtain a water reward in either arm in the choice period. During the DNMS training period, mice obtain water only in the non-matched arm in the choice period.

$$\begin{aligned}&\textit{Percentage of choosing the nonmatch arm}\\&=\textit{number of the trials in which the nonmatched}\\&\quad\textit{arm was chosen}/\textit{total number of trials}\times 100\%.\end{aligned}$$

In the task training phase, the correct performance rate (referred to as "performance" in the figure legends) was calculated per day.

Results

Overview of the Hardware, Software, and Automatic Training Protocol

The HASS allowed fully-automatic training. The events of mice passing by at different locations were detected by infrared sensors and registered by the program built into the Arduino motherboard. The Arduino-based control unit sent control signals to trigger the following processes: door opening and closing driven by servos, and water delivery by peristaltic pumps (Fig. 3). The embedded round acrylic plate controlled by a servo rotated by a random angle during the delay period to remove traces of a previous visit. The only steps human operators needed to perform were the preparation before training and cleaning the equipment after training.

To minimize human intervention during the entire training process, we developed a step-by-step training protocol. The protocol included one preparatory step (habituation) and two training phases (shaping and task-learning, Fig. 6). The naïve mice were automatically trained with this protocol. All of the mice performed the spatial DNMS task at a stable level after training (see below).

The first step of training was shaping (Figs. 6, 7A) the "come-back" rule, which had the following three aims: (1) to train the mice to run back to the home arm after exploring the goal arms; (2) to teach mice to obtain a water reward delivered at the end of each arm; and (3) to allow mice to be familiar with the closing/opening of the doors. On the first day of shaping, all mice quickly learned to drink the water delivered from the water port within several trials. They still spent some time exploring other closed doors between the goal and home arms during this step. The mice were expected to complete at least 50 trials in 2 h. The daily shaping phase ended when the mice performed 60 trials or the training lasted more than 2 h. This phase lasted for 3–5 days.

The following step was the DNMS task training phase (Figs. 6, 8A). During this phase, the mice had to remember

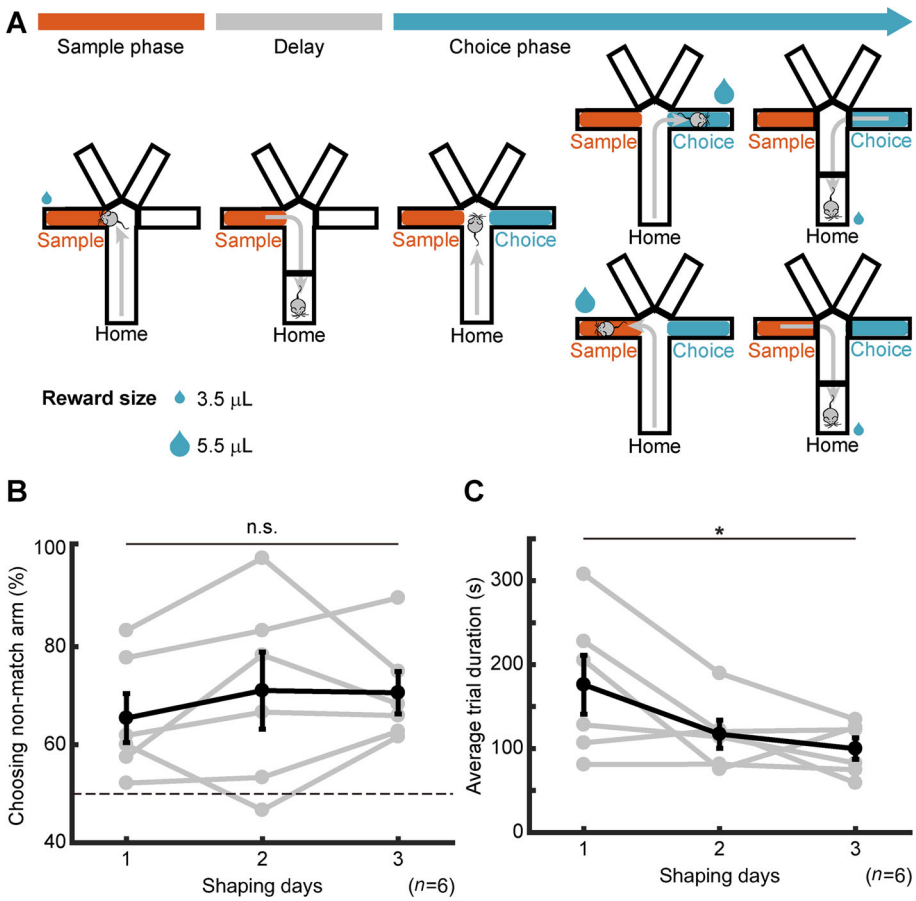

Fig. 7 Behavioral results for shaping. **A** Schematics of the behavioral design for shaping, showing one example trial with a "T" arm configuration. **B** Rate of choosing the nonmatched arm in the shaping phase; each gray curve represents one mouse and the black curve represents the mean value for all mice (two-way ANOVA, main effect of nonmatched arm preference, $F(1, 30) = 61.58$, $P < 0.001$; effect of days, $F(2, 30) = 0$, $P = 1$; interaction effect, $F(2, 30) = 0.55$, $P = 0.58$). **C** Average time to finish one trial (repeated measures ANOVA, $F(2, 10) = 6.06$, $P = 0.019$; gray curves represent single cases, black curve represents average data).

the information of the sampled arm and enter the nonmatched arm in the choice phase to obtain a water reward. Two types of sessions were designed: normal and teaching sessions. In the normal session, the sample and choice arms were pseudo randomly chosen and varied from trial to trial. In this session, the number of trials was balanced for all the sample and choice arms. In the teaching session, error-correction trials were applied if the mice consistently made errors. In the error-correction trials, the sample arm of the last trial was repeated until the mouse completed a hit trial. The training started with a normal session and switched to a teaching session when mice performed at low accuracy (<65%) and exhibited no increase on consecutive days. After training, mice performed the DNMS task at a stable level.

Mice Showed a Preference for the Nonmatched Arm in the Shaping Phase

We trained 6 naive mice to perform the spatial DNMS task. Before task training, mice underwent behavioral shaping (Fig. 7A). Although mice were allowed to make free choices in this phase, the rate of choosing the nonmatched arm was higher than chance [day 1 (mean ± SD), 65.4± 12.3%; day 2, 71.1 ± 19.3%; day 3, 70.6 ± 10.6%, $P = 0.031$]. Two-way ANOVA yielded a main effect for the nonmatched arm preference, $F(1, 30) = 61.58$, $P < 0.001$, such that the average rate of choosing the nonmatched arm was significantly higher than that of choosing a matched arm. The main effect of days was not significant, $F(2, 30) = 0$, $P = 1$, indicating that such a preference was stable across days. The interaction effect was not significant, $F(2, 30) = 0.55$, $P = 0.581$(Fig. 7B, two-way ANOVA). This phenomenon is consistent with the idea that rodents are likely to use a win-switch strategy in foraging [55–62].

At the beginning of shaping, the mice explored other closed doors or entered the same arm repeatedly. The average time per trial was >150 s on day 1 of shaping (176 ± 86 s), and most of the mice could not complete 60 trials in 2 h. After shaping for 3 days, the average duration of each trial decreased (day 2, 117 ± 41 s; day 3, 100 ± 32 s). The main effect of training yielded an F ratio of $F(2, 10) = 6.06$, $P = 0.019$ (Fig. 7C, repeated measures ANOVA), indicating that the mice were already familiar with the "come-back" rule and ready for DNMS task training.

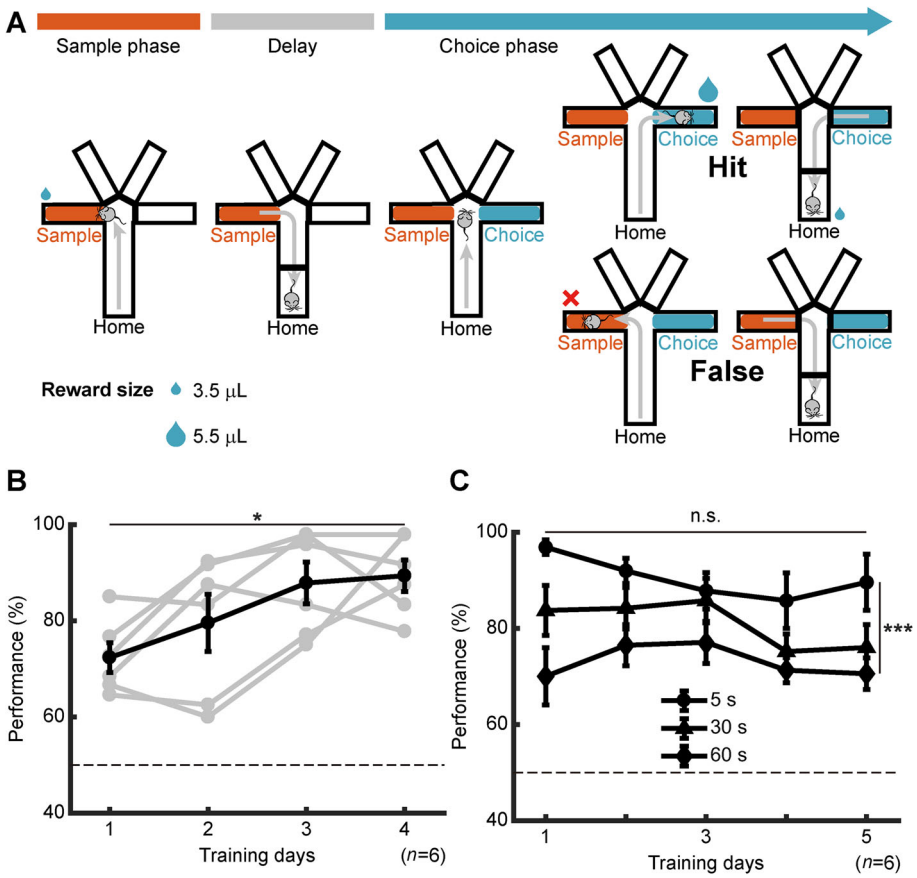

Fig. 8 Behavioral results of the DNMS task. **A** Schematics of the behavioral design for the DNMS task, showing one example trial with a "T" arm configuration. **B** Performance of mice in the DNMS task with the delay fixed at 5 s. Gray curves represent different mice; black curve represents averaged performance across mice (repeated measures ANOVA, $F(3, 15) = 5.17$, $P = 0.012$). **C** Performance of mice in the DNMS task with different delays (mixed two-way ANOVA, delay effect, $F(2, 15) = 22.11$, $P < 0.001$; training effect, $F(4, 60) = 1.55$, $P = 0.200$).

Training for the DNMS Task

After shaping, the mice underwent training for the DNMS task in the HASS. In the first 4 days, the delay was fixed at 5 s, and the intertrial interval was 10 s. In this design, the mouse had to temporally maintain the information of the location of the sampled arm during the delay period (Fig. 8A). Consistent with their preference for a non-matched arm, as shown in the shaping phase, the performance on day 1 of training was above chance level (50%). The main effect of training yielded an F ratio of $F(3, 15) = 5.17$, $P = 0.012$, indicating that the performance significantly increased after the 4 days of training (Fig. 8B, repeated measures ANOVA). The total number of trials completed in 4 days was ~240.

In the following days, the mice were trained to perform the DNMS task with varying delays. Compared with the fixed-delay version, the task structure was the same but delay varied among 5 s, 30 s, and 60 s. The trial number at each delay was balanced. The main effect of delay duration yielded an F ratio of $F(2, 15) = 22.11$, $P < 0.001$, indicating that mice performed better in 5-s delay trials (91.8 ± 8.7%) than in trials at a 30-s (75.0 ± 12.7%) or 60-s delay (68.7 ± 12.9%). However, the main effect of different days yielded an F ratio of $F(4, 60) = 1.55$, $P = 0.200$, indicating that the performance for each condition was stable during 5 days of training (Fig. 7C, mixed two-way ANOVA).

Discussion

A suitable behavioral paradigm is the key to understanding the mechanisms underlying cognitive functions. Moreover, an optimized training system can improve data quality as well as training efficiency. Here, we presented the HASS, an automatic system with four choice arms for training spatial cognitive behaviors in free-moving mice. More arms than the traditional T-maze and Y-maze were added, which allowed more flexibility in the behavioral design, allowing the study of other brain functions. For example, the behavioral rule can be different in the different "T" and "Y" arms in our system. Therefore, one can easily study the neural mechanisms underlying rule-switching.

To decrease human bias during behavioral experiments as well as increase efficiency, we developed this training system, which allows fully automatic training. Human operators only needed to test and adjust the training units before and after training, gently put mice in the home arm, close the light-blocking curtain, select and run computer

software controlling the training protocols, run the monitor, and retrieve the mice after training was complete. There were benefits from using the automatic training system and training protocol, and human intervention was minimized. Mice could be trained in different systems simultaneously in a short period, thus increasing efficiency. With this explicit training protocol, behavioral results from different operators or labs are comparable.

The stress level of the mice was minimized by removing human intervention from the entire session, minimizing the chance of getting hit by an opening/closing door, and reducing the ambient noise in shaping sessions.

A current limitation is that the HASS monitors only the mouse-passage events as behavioral readouts. To obtain a deeper understanding of the behavior and underlying neural circuit, one would also like to integrate more monitoring systems for behavioral events, such as head direction [63, 64], movement speed [65], trace, and animal position [6, 7, 66]. Aside from the infrared signal, the recorded video could be used to analyze these behavioral events.

Another limitation is that the number of daily training trials was limited to 60, which could be a shortcoming under various trial conditions (for instance, varying delay durations and the catch-trial design of optogenetic perturbation). Fortunately, the performance of mice was stable after a thorough training period (Fig. 7B, C), allowing cross-day data accumulation during a long training process.

The HASS allows automated training of spatial behaviors in free-moving mice. Our design also supports high-throughput behavioral screening. In summary, the current system is a good choice for circuitry studies of spatial behavior.

Acknowledgements The work was supported by the Instrument Developing Project of the Chinese Academy of Sciences (YZ201540), the National Science Foundation for Distinguished Young Scholars of China (31525010), the General Program of the National Science Foundation of China (31471049), the Key Research Project of Frontier Science of the Chinese Academy of Sciences (QYZDB-SSW-SMC009), China – Netherlands CAS-NWO Programme: Joint Research Projects, The Future of Brain and Cognition (153D31KYSB20160106), the Key Project of Shanghai Science and Technology Commission (15JC1400102, 16JC1400101), and the State Key Laboratory of Neuroscience, China. We thank Xuehan Zhou and Dr. Ding Liu for assistance with designing the system and for training protocol optimization, and Dr. Xiaoxing Zhang for suggestions about programming.

References

1. Gomez-Marin A, Paton JJ, Kampff AR, Costa RM, Mainen ZF. Big behavioral data: psychology, ethology and the foundations of neuroscience. Nat Neurosci 2014, 17: 1455–1462.
2. Baddeley A. Working memory: theories, models, and controversies. Annu Rev Psychol 2012, 63: 1–29.
3. Bai W, Liu T, Yi H, Li S, Tian X. Anticipatory activity in rat medial prefrontal cortex during a working memory task. Neurosci Bull 2012, 28: 693–703.
4. Gold JI, Shadlen MN. The neural basis of decision making. Annu Rev Neurosci 2007, 30: 535–574.
5. Lee D, Seo H, Jung MW. Neural basis of reinforcement learning and decision making. Annu Rev Neurosci 2012, 35: 287–308.
6. O'Keefe J, Dostrovsky J. The hippocampus as a spatial map. Preliminary evidence from unit activity in the freely-moving rat. Brain Res 1971, 34: 171–175.
7. Fyhn M, Molden S, Witter MP, Moser EI, Moser MB. Spatial representation in the entorhinal cortex. Science 2004, 305: 1258–1264.
8. Wood RA, Bauza M, Krupic J, Burton S, Delekate A, Chan D, *et al.* The honeycomb maze provides a novel test to study hippocampal-dependent spatial navigation. Nature 2018, 554: 102–105.
9. Fernando AB, Robbins TW. Animal models of neuropsychiatric disorders. Annu Rev Clin Psychol 2011, 7: 39–61.
10. Gotz J, Ittner LM. Animal models of Alzheimer's disease and frontotemporal dementia. Nat Rev Neurosci 2008, 9: 532–544.
11. Nestler EJ, Hyman SE. Animal models of neuropsychiatric disorders. Nat Neurosci 2010, 13: 1161–1169.
12. Schaefer AT, Claridge-Chang A. The surveillance state of behavioral automation. Curr Opin Neurobiol 2012, 22: 170–176.
13. Fenno L, Yizhar O, Deisseroth K. The development and application of optogenetics. Annu Rev Neurosci 2011, 34: 389–412.
14. Armbruster BN, Li X, Pausch MH, Herlitze S, Roth BL. Evolving the lock to fit the key to create a family of G protein-coupled receptors potently activated by an inert ligand. Proc Natl Acad Sci U S A 2007, 104: 5163–5168.
15. Deisseroth K, Schnitzer MJ. Engineering approaches to illuminating brain structure and dynamics. Neuron 2013, 80: 568–577.
16. Davidson AB, Davis DJ, Cook L. A rapid automatic technique for generating operant key-press behavior in rats. J Exp Anal Behav 1971, 15: 123–127.
17. Benkner B, Mutter M, Ecke G, Munch TA. Characterizing visual performance in mice: an objective and automated system based on the optokinetic reflex. Behav Neurosci 2013, 127: 788–796.
18. de Visser L, van den Bos R, Spruijt BM. Automated home cage observations as a tool to measure the effects of wheel running on cage floor locomotion. Behav Brain Res 2005, 160: 382–388.
19. Kretschmer F, Kretschmer V, Kunze VP, Kretzberg J. OMR-arena: automated measurement and stimulation system to determine mouse visual thresholds based on optomotor responses. PLoS One 2013, 8: e78058.
20. Han Z, Zhang X, Zhu J, Chen Y, Li CT. High–throughput automatic training system for odor-based learned behaviors in head-fixed mice. Front Neural Circuits 2018, 12.
21. Kazdoba TM, Del Vecchio RA, Hyde LA. Automated evaluation of sensitivity to foot shock in mice: inbred strain differences and pharmacological validation. Behav Pharmacol 2007, 18: 89–102.
22. Roughan JV, Wright-Williams SL, Flecknell PA. Automated analysis of postoperative behaviour: assessment of HomeCageScan as a novel method to rapidly identify pain and analgesic effects in mice. Lab Anim 2009, 43: 17–26.
23. Anagnostaras SG, Wood SC, Shuman T, Cai DJ, Leduc AD, Zurn KR, *et al.* Automated assessment of pavlovian conditioned freezing and shock reactivity in mice using the video freeze system. Front Behav Neurosci 2010, 4.
24. Kopec CD, Kessels HW, Bush DE, Cain CK, LeDoux JE, Malinow R. A robust automated method to analyze rodent motion during fear conditioning. Neuropharmacology 2007, 52: 228–233.

25. Balci F, Oakeshott S, Shamy JL, El-Khodor BF, Filippov I, Mushlin R, *et al.* High-throughput automated phenotyping of two genetic mouse models of Huntington's disease. PLoS Curr 2013, 5.
26. Jhuang H, Garrote E, Mutch J, Yu X, Khilnani V, Poggio T, *et al.* Automated home-cage behavioural phenotyping of mice. Nat Commun 2010, 1: 68.
27. Hubener J, Casadei N, Teismann P, Seeliger MW, Bjorkqvist M, von Horsten S, *et al.* Automated behavioral phenotyping reveals presymptomatic alterations in a SCA3 genetrap mouse model. J Genet Genomics 2012, 39: 287–299.
28. Aarts E, Maroteaux G, Loos M, Koopmans B, Kovacevic J, Smit AB, *et al.* The light spot test: Measuring anxiety in mice in an automated home-cage environment. Behav Brain Res 2015, 294: 123–130.
29. Adamah-Biassi EB, Stepien I, Hudson RL, Dubocovich ML. Automated video analysis system reveals distinct diurnal behaviors in C57BL/6 and C3H/HeN mice. Behav Brain Res 2013, 243: 306–312.
30. Hong W, Kennedy A, Burgos-Artizzu XP, Zelikowsky M, Navonne SG, Perona P, *et al.* Automated measurement of mouse social behaviors using depth sensing, video tracking, and machine learning. Proc Natl Acad Sci U S A 2015, 112: E5351–5360.
31. Weissbrod A, Shapiro A, Vasserman G, Edry L, Dayan M, Yitzhaky A, *et al.* Automated long-term tracking and social behavioural phenotyping of animal colonies within a semi-natural environment. Nat Commun 2013, 4: 2018.
32. Ohayon S, Avni O, Taylor AL, Perona P, Roian Egnor SE. Automated multi-day tracking of marked mice for the analysis of social behaviour. J Neurosci Methods 2013, 219: 10–19.
33. Reiss D, Walter O, Bourgoin L, Kieffer BL, Ouagazzal AM. New automated procedure to assess context recognition memory in mice. Psychopharmacology (Berl) 2014, 231: 4337–4347.
34. Remmelink E, Loos M, Koopmans B, Aarts E, van der Sluis S, Smit AB, *et al.* A 1-night operant learning task without food-restriction differentiates among mouse strains in an automated home-cage environment. Behav Brain Res 2015, 283: 53–60.
35. Becker AM, Meyers E, Sloan A, Rennaker R, Kilgard M, Goldberg MP. An automated task for the training and assessment of distal forelimb function in a mouse model of ischemic stroke. J Neurosci Methods 2016, 258: 16–23.
36. Erlich JC, Bialek M, Brody CD. A cortical substrate for memory-guided orienting in the rat. Neuron 2011, 72: 330–343.
37. Poddar R, Kawai R, Olveczky BP. A fully automated high-throughput training system for rodents. PLoS One 2013, 8: e83171.
38. Gallistel CR, Balci F, Freestone D, Kheifets A, King A. Automated, quantitative cognitive/behavioral screening of mice: for genetics, pharmacology, animal cognition and undergraduate instruction. J Vis Exp 2014: e51047.
39. Romberg C, Horner AE, Bussey TJ, Saksida LM. A touch screen-automated cognitive test battery reveals impaired attention, memory abnormalities, and increased response inhibition in the TgCRND8 mouse model of Alzheimer's disease. Neurobiol Aging 2013, 34: 731–744.
40. Spellman T, Rigotti M, Ahmari SE, Fusi S, Gogos JA, Gordon JA. Hippocampal-prefrontal input supports spatial encoding in working memory. Nature 2015, 522: 309–314.
41. Hanks TD, Kopec CD, Brunton BW, Duan CA, Erlich JC, Brody CD. Distinct relationships of parietal and prefrontal cortices to evidence accumulation. Nature 2015, 520: 220–223.
42. Brunton BW, Botvinick MM, Brody CD. Rats and humans can optimally accumulate evidence for decision-making. Science 2013, 340: 95–98.
43. Fuster JM. The prefrontal cortex : anatomy, physiology, and neuropsychology of the frontal lobe. 3rd ed. Philadelphia: Lippincott-Raven, 1997.
44. Smith EE, Jonides J. Storage and executive processes in the frontal lobes. Science 1999, 283: 1657–1661.
45. D'Esposito M, Postle BR. The cognitive neuroscience of working memory. Annu Rev Psychol 2015, 66: 115–142.
46. Goldman-Rakic PS. Cellular basis of working memory. Neuron 1995, 14: 477–485.
47. Lewis DA, Gonzalez-Burgos G. Pathophysiologically based treatment interventions in schizophrenia. Nat Med 2006, 12: 1016–1022.
48. Ito HT, Zhang SJ, Witter MP, Moser EI, Moser MB. A prefrontal-thalamo-hippocampal circuit for goal-directed spatial navigation. Nature 2015, 522: 50–55.
49. Bolkan SS, Stujenske JM, Parnaudeau S, Spellman TJ, Rauffenbart C, Abbas AI, *et al.* Thalamic projections sustain prefrontal activity during working memory maintenance. Nat Neurosci 2017, 20: 987–996.
50. Yamamoto J, Suh J, Takeuchi D, Tonegawa S. Successful execution of working memory linked to synchronized high-frequency gamma oscillations. Cell 2014, 157: 845–857.
51. Kolb B, Nonneman AJ, Singh RK. Double dissociation of spatial impairments and perseveration following selective prefrontal lesions in rats. J Comp Physiol Psychol 1974, 87: 772–780.
52. Baeg EH, Kim YB, Huh K, Mook-Jung I, Kim HT, Jung MW. Dynamics of population code for working memory in the prefrontal cortex. Neuron 2003, 40: 177–188.
53. Fujisawa S, Amarasingham A, Harrison MT, Buzsaki G. Behavior-dependent short-term assembly dynamics in the medial prefrontal cortex. Nat Neurosci 2008, 11: 823–833.
54. Sigurdsson T, Stark KL, Karayiorgou M, Gogos JA, Gordon JA. Impaired hippocampal-prefrontal synchrony in a genetic mouse model of schizophrenia. Nature 2010, 464: 763–767.
55. Pioli EY, Gaskill BN, Gilmour G, Tricklebank MD, Dix SL, Bannerman D, *et al.* An automated maze task for assessing hippocampus-sensitive memory in mice. Behav Brain Res 2014, 261: 249–257.
56. Rawlins JN, Maxwell TJ, Sinden JD. The effects of fornix section on win-stay/lose-shift and win-shift/lose-stay performance in the rat. Behav Brain Res 1988, 31: 17–28.
57. McDaniel WF, Jones PD, Weaver TL. Medial frontal lesions, postoperative treatment with an ACTH(4–9) analog, and acquisition of a win-shift spatial strategy. Behav Brain Res 1991, 44: 107–112.
58. Ritzmann RF, Kling A, Melchior CL, Glasky AJ. Effect of age and strain on working memory in mice as measured by win-shift paradigm. Pharmacol Biochem Behav 1993, 44: 805–807.
59. Randall CK, Zentall TR. Win-stay/lose-shift and win-shift/lose-stay learning by pigeons in the absence of overt response mediation. Behav Processes 1997, 41: 227–236.
60. Sage JR, Knowlton BJ. Effects of US devaluation on win-stay and win-shift radial maze performance in rats. Behav Neurosci 2000, 114: 295–306.
61. Taylor CL, Latimer MP, Winn P. Impaired delayed spatial win-shift behaviour on the eight arm radial maze following excitotoxic lesions of the medial prefrontal cortex in the rat. Behav Brain Res 2003, 147: 107–114.
62. Olton DS, Schlosberg P. Food-searching strategies in young rats: Win-shift predominates over win-stay. J Comp Physiol Psychol 1978, 92: 609–618.
63. Taube JS, Muller RU, Ranck JB, Jr. Head-direction cells recorded from the postsubiculum in freely moving rats. I. Description and quantitative analysis. J Neurosci 1990, 10: 420–435.
64. Taube JS, Muller RU, Ranck JB, Jr. Head-direction cells recorded from the postsubiculum in freely moving rats. II. Effects of environmental manipulations. J Neurosci 1990, 10: 436–447.
65. Kropff E, Carmichael JE, Moser MB, Moser EI. Speed cells in the medial entorhinal cortex. Nature 2015, 523: 419–424.
66. Hafting T, Fyhn M, Molden S, Moser MB, Moser EI. Microstructure of a spatial map in the entorhinal cortex. Nature 2005, 436: 801–806.